XL CILAMCE
IBERO-LATIN AMERICAN CONGRESS ON COMPUTATIONAL METHODS IN ENGINEERING
NOVEMBER 11-14, 2019
Praiamar Natal Hotel & Convention
Natal, RN-BRAZIL

AN EFFICIENT LOCKING-FREE COROTATIONAL BEAM FINITE ELEMENT

Jéssica G. S. A. Meireles
Regiane P. de Barros
Eliseu Lucena Neto
Francisco A. C. Monteiro
jessicagmeireles@gmail.com
regianefp@hotmail.com
eliseu@ita.br
facm@ita.br
Instituto Tecnológico de Aeronáutica
Praça Marechal Eduardo Gomes, 50, 12228-900, São José dos Campos, SP, Brazil

Abstract. An efficient and accurate locking-free corotational beam finite element is developed in this work. The element is locally linear, with the displacement varying according to the Timoshenko assumption and the difference of electric potential varying linearly through each piezoelectric layer thickness. The shape functions are appropriately derived from the exact solution of the homogeneous form of the linear equilibrium equations written in terms of displacements, rotations and differences of electric potential. Since the resulting 2-node element has the same degrees of freedom as the associated purely mechanical beam element (two displacements and one rotation per node), it can be directly plugged into an element-independent corotational algorithm to suitably analyze piezoelectric plane frames under small strains but large rotations. A consistent incremental-iterative technique based on the Newton-Raphson method is employed for the solution of the nonlinear equilibrium equations. Numerical examples that demonstrate the efficiency and large rotation capability of the corotational formulation are presented. The element results are validated by exact solutions available in the literature. Very good agreement is found in all cases.

Keywords: Piezoelectric beam, Corotational model, Finite element

1 Introduction

Smart materials are those that exhibit some type of coupling between different physical domains and may have their characteristics modified by controlled changes of state variables that characterize the mechanical, electrical, thermal and chemical domains, for example. Thus, piezoelectric materials are classified as smart because they exhibit coupling between the mechanical and electrical domains [1]. Piezoelectrics, available in the form of thin sheets of ceramic or polymer, are the most popular and practical smart materials due to their coupled electromechanical properties, that make them suitable for use as distributed sensors and actuators to control structural response.

In the sensor application, strains can be determined from measurements of induced electric potential (direct piezoelectric effect), whereas in actuator applications strains can be controlled through the input of appropriate electric potential (converse piezoelectric effect). The technology of self-monitoring and self-controlling smart structures, by integrating distributed piezoelectric sensors and actuators, provides the possibility for the development of light-weight and rigid structures.

Linear analysis of smart structures is much more widespread in the literature than the more sophisticated non-linear analysis [2]. However, the contribution of geometric nonlinearities may be crucial because external excitations can lead to this type of structure at high rotations, even under small strains, given its inherent flexibility [3]. Therefore, a linear analysis may be insufficient to accurately estimate the voltage measured by the piezoelectric sensors [3,4,5], impairing the control of these structures by the restorative voltage to be provided in the actuators. Non-linear models of piezoelectric beams under large rotations (but not totally unrestricted) are more widespread in the literature [4-6] than models with free restriction rotations [2].

Structures under geometric nonlinearity caused by large rotations, but restricted to small strains, can be described by the corotational formulation, as explained below. The motion of a solid in space is illustrated in Fig. 1, for didactic purposes, by a clamped–free beam divided into four finite elements and subjected to a moment-load. Suppose we want to determine the configuration C_n of the element near the free end when the acting load has magnitude M_n. The non-linear nature of the problem requires that the solution be obtained in steps: we know the configurations C_0, C_1, … , C_{n-1} to then determine the configuration C_n. Four of these configurations are indicated in Fig. 1: the initial configuration C_0, an intermediate configuration C_i, the configuration C_{n-1} and the current configuration C_n to be determined.

If in the incremental-iterative process for the determination of C_n the equations are established by reference to a known configuration, a Lagrangian description is being used: in the total Lagrangian description C_0 is the reference configuration; in the updated Lagrangian description the reference is the C_{n-1} configuration. Cescotto *et al.* [7] suggest the 'generalized' name for the description with reference in an intermediate configuration C_i, which has as particular cases the total Lagrangian description ($C_i = C_0$) and the updated one ($C_i = C_{n-1}$). The Eulerian description, which would use the C_n configuration itself as a reference, has limited use in the mechanics of solids because C_n is an unknown configuration in the solution process. In geometrically linear problems, the use of the total Lagrangian description is tacit due to the proximity between C_0 and C_n.

For large rotations under small strains, the corotational finite elements have shown a certain superiority comparing to the elements that use Lagrangian descriptions. Such elements adopt an undeformed auxiliary configuration C_{0n}, very close to the C_n, which is obtained exclusively by the rigid-body motion of the element of its configuration C_0. No portion of rigid-body motion exists between the C_{0n} and C_n configurations so that any displacement between these configurations is converted into strain. To identify C_{0n} with this property would be ideal for the corotational description, which has its origin in the polar decomposition theorem [8,9]. Using both configurations C_0 and C_{0n} as a reference, the corotational description can not, strictly speaking, be classified as Lagrangian or Eulerian, as it sometimes appears labeled in the literature.

For a better understanding of why the simultaneous use of the C_0 and C_{0n} configurations is so essential to the success of the corotational finite elements, realize that we can approximate C_{0n} of C_n

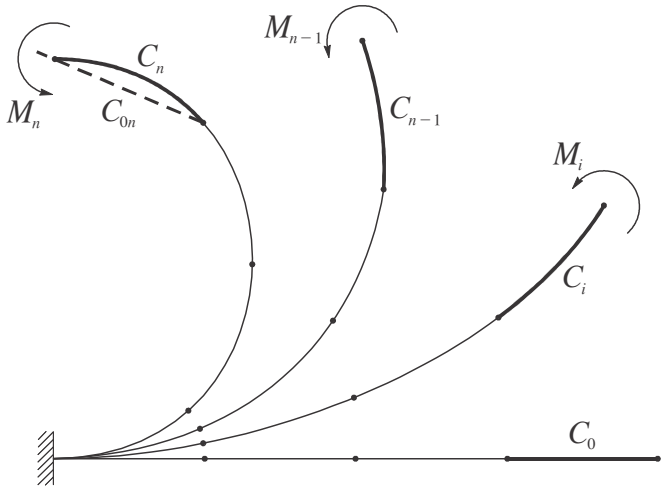

Figure 1. Equilibrium configurations C_0, C_i, C_n and auxiliary configuration C_{0n}

as much as we want by reducing the size of the element with the refinement of the mesh. Since strain is measured relative to C_{0n}, and not to C_0 as it does, for example, the total Lagrangian formulation [10], we can adopt a simple linear element to describe the motion between C_{0n} and C_n. All the geometric non-linearity that occurs in the complete motion between C_0 and C_n is excluded from the local formulation (between C_{0n} and C_n) of the element. It is the relationship that we establish between the nodal displacement increments between the C_{0n} and C_n configurations and the C_0 and C_n configurations that will account for the geometric nonlinearity in the formulation.

Argyris [11] was a pioneer in the formulation of finite elements that is based on the decomposition of the movement in the rigid portion and in the one that produces strain. This 'natural approach', as it has come to be called, is described in detail in [12]. Similar ideas were also used by Wempner [13], Belytschko and Hsieh [14], Oran [15-16] and Oran and Kassimali [17]. It is in the work of Belytschko and Glaum [18] that the name 'corotational' appears for the first time to designate the existence of a local system of axes that moves and rotates continuously with the element. Since then, most of the articles published on the subject have adopted this terminology.

Using a total Lagrangian description, Mukherjee and Chaudhuri [4,5] propose nonlinear finite element models for piezoelectric beams under large rotations, but not totally unrestricted. In a similar description, Cardoso and Fonseca [2] bring a rigorous treatment of geometric non-linearity and show examples of beams and plane frames using a piezoelectric version of the isoparametric 8-node element under plane stress found in [19]. Differently from those who deal with a corotational formulation, in the work of [2], the measurements of stress, strain and electrical quantities are carefully defined about the C_0 configuration taking into consideration large transformations.

Although we have not found in the literature any corotational model of piezoelectric beams, we find the works of Rama *et al.* [20] and Marinković and Rama [21] about corotational models of piezoelectric shells. They are emphatic in drawing attention to the difficulty of considering strictly the follower nature of the load induced by actuators, where both the direction and the intensity of the load changes with each new configuration of the structure. They suggest, based on recommendations by [19], that the solution of the nonlinear problem be done in small increments accompanied by the appropriate updating of this type of load to obtain sufficiently precise results.

We developed in this paper a corotational model of finite elements for piezoelectric plane frames. A linear element is proposed to describe the motion between the C_{0n} and C_n configurations, whose displacement varies according to Timoshenko assumption and the electric potential has linear variation along with the thickness of each piezoelectric layer. Unlike [2], the proximity between C_{0n} and C_n configurations avoids the use of far-reaching measures of stress, strain and other quantities, thus justifying the adoption of the linear element. The interpolation functions of the element are identified from the general solution of the homogeneous part of the system of equations that describes the linear problem. Therefore, it is a superconvergent element [22-24]. That is, the element can provide exact nodal results for mechanical quantities (displacement, rotation and stresses) in linear static problems,

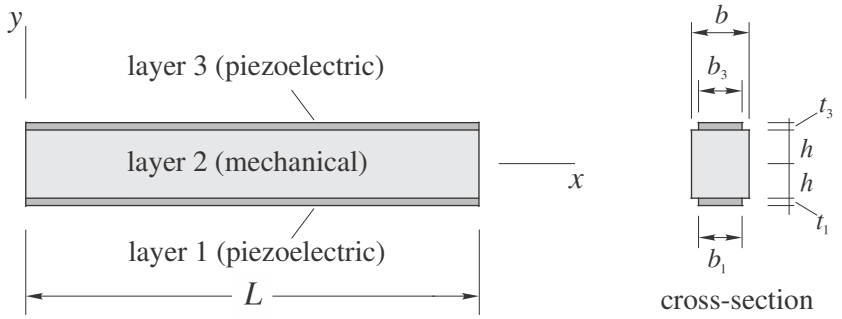

Figure 2. Timoshenko beam configuration

regardless of the number of elements used in the mesh or applied loads. Nothing is yet known about the accuracy of the electrical quantities obtained by such a type of element.

Since the proposed element has two nodes, with the same degrees of freedom of the corresponding purely mechanical element (two displacements and one rotation per node), it can be easily inserted into a corotational algorithm that enables it to deal with piezoelectric plane frames under large rotations, but small strains. Thus, any additional complexity brought about by piezoelectricity is treated locally. An incremental-iterative approach based on the Newton- Raphson method is then employed for the solution of the nonlinear discrete problem. Contrary to the procedure adopted by [20,21], all the linearizations required by the Newton-Raphson method are analytically and consistently formulated, including those related to the follower nature of the piezoelectrically induced loads. Numerical examples illustrate the efficiency of the developed model.

2 Fundamentals

The beam of length L shown in Fig 2 has a pure mechanical core layer (width b, thickness $2h$), and continuous piezoelectric layers attached with at the bottom (width b_1, thickness t_1) and at the top (width b_3, thickness t_3) of the beam. Under the linear kinematic assumptions of Timoshenko formulation, the displacement components of any (particle) point on the beam can be found by

$$u_x(x,y) = u(x) + y\beta(x) \qquad u_y(x,y) = v(x) \tag{1}$$

where $u(x)$, $v(x)$ are the axis displacements in the x, y directions, and $\beta(x)$ is the rotation of the cross-section. The potential value along the bottom $(k = 1)$ and top $(k = 3)$ of each piezoelectric layer may be expressed assuming a linear map [25]

$$\phi(x,y) = \left(1 - \frac{y-y_k}{t_k}\right)\phi_k(x) + \frac{y-y_k}{t_k}\phi_{k+1}(x) \tag{2}$$

through the thickness, where $\phi_k(x)$ and $\phi_{k+1}(x)$ are the potential value at the bottom of the k-layer $(y = y_k)$ and at its top $(y = y_{k+1} = y_k + t_k)$ respectively.

According Santos [10], the principle of virtual work applied to the beam depicted in Fig 3 states that

$$\begin{aligned} &-\int_0^L (N\delta\epsilon_m + M\delta\kappa + Q\delta\gamma + L_1\delta\bar{\phi}_1 + L_3\delta\bar{\phi}_3)dx \\ &+\int_0^L \left(q_x\delta u + q_y\delta v\right)dx + \sum_{i=1}^2 \left(F_{xi}\delta u_i + F_{yi}\delta v_i + M_i\delta\theta_i\right) = 0 \end{aligned} \tag{3}$$

with the generalized strains

$$\epsilon_m = u' \qquad \kappa = \beta' \qquad \gamma = v' + \beta \qquad \bar{\phi}_k = (\phi_{k+1} - \phi_k)/t_k \tag{4}$$

being the energy conjugates of the generalized stresses N, M, Q, L_k; the quantity $\theta_i = -\beta_i$; and a comma indicates differentiation with respect to x. Constitutive relations can be expressed in the form

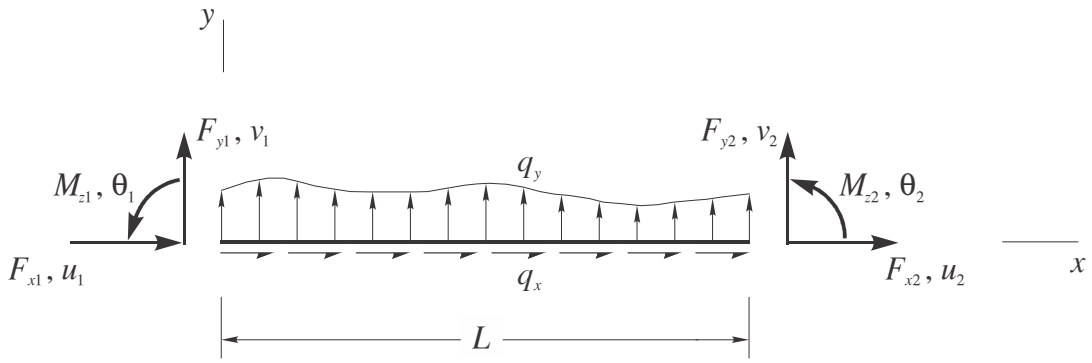

Figure 3. Free-body beam diagram

$$\begin{Bmatrix} N \\ M \\ Q \\ L_1 \\ L_3 \end{Bmatrix} = \begin{bmatrix} A_{11} & A_{12} & 0 & A_{14} & A_{15} \\ & A_{22} & 0 & A_{24} & A_{25} \\ & & A_{33} & 0 & 0 \\ & \text{sym} & & A_{44} & 0 \\ & & & & A_{55} \end{bmatrix} \begin{Bmatrix} \epsilon_m \\ \kappa \\ \gamma \\ \bar{\phi}_1 \\ \bar{\phi}_3 \end{Bmatrix} \tag{5}$$

with constants A_{ij} involving both geometry and material properties of the beam layers. Their values can vary depending on the constitutive model version. Herein, on assume the version adopted by [26-29]. Explicit expressions for the entries A_{ij} can be found in [10,30].

After integration by parts of Eq. (3), the fundamental lemma of variational calculus [31] leads to

$$N' + q_x = 0 \qquad Q' + q_y = 0 \qquad M' - Q = 0 \qquad L_1 = 0 \qquad L_3 = 0 \tag{6}$$

in $0 < x < L$. In these relations, equations involving the quantities N, M, Q establish the mechanical equilibrium of the beam whereas the remaining ones state the Gauss law for each piezoelectric layer.

3 Finite Element

3.1 Superconvergent formulation

The foremost requirement for formulating a superconvergent element is to derive its shape functions. Following [22-24], such functions can be identified from the general solution of

$$N' = 0 \qquad Q' = 0 \qquad M' - Q = 0 \qquad L_1 = 0 \qquad L_3 = 0 \tag{7}$$

which are the homogeneous part of Eq. (6), i.e., the governing differential equations of the associated linear problem. Substitution of Eq. (5) and Eq. (4) into Eq. (7), and integrating the resulting relations yields

$$\begin{aligned} A_{11}u' + A_{12}\beta' + A_{14}\bar{\phi}_1 + A_{15}\bar{\phi}_3 &= c_1 \\ A_{33}(v' + \beta) &= c_2 \\ A_{12}u' + A_{22}\beta' + A_{24}\bar{\phi}_1 + A_{25}\bar{\phi}_3 &= c_2 x + c_3 \\ A_{14}u' + A_{24}\beta' + A_{44}\bar{\phi}_1 &= 0 \\ A_{15}u' + A_{25}\beta' + A_{55}\bar{\phi}_3 &= 0 \end{aligned} \tag{8}$$

where c_i are integration constants.

If the bottom/top layers are piezoelectric actuators then the last two equations of the governing differential system vanish, and the respective prescribed electric potential differences $\bar{\phi}_1$, $\bar{\phi}_3$ are known quantities. In this way, one can accordingly rewrite Eq. (8) in the form

$$\begin{aligned} A_{11}u' + A_{12}\beta' + C_1A_{14}\bar{\phi}_1 + C_3A_{15}\bar{\phi}_3 &= c_1 - \phi_u \\ A_{33}(v' + \beta) &= c_2 \\ A_{12}u' + A_{22}\beta' + C_1A_{24}\bar{\phi}_1 + C_3A_{25}\bar{\phi}_3 &= c_2x + c_3 - \phi_\beta \\ C_1(A_{14}u' + A_{24}\beta' + A_{44}\bar{\phi}_1) &= 0 \\ C_3(A_{15}u' + A_{25}\beta' + A_{55}\bar{\phi}_3) &= 0 \end{aligned} \tag{9}$$

If a piezoelectric layer k has a sensing configuration then $C_k = 1$, else $C_k = 0$. A sensing layer configuration is consistently taken into account by introducing the relations derived from Gauss law into the left hand side (LHS) of equilibrium equations, and setting to unity the respective control parameter C_k. The terms

$$\begin{aligned} \phi_u &= (1 - C_1)A_{14}\bar{\phi}_1 + (1 - C_3)A_{15}\bar{\phi}_3 \\ \phi_\beta &= (1 - C_1)A_{24}\bar{\phi}_1 + (1 - C_3)A_{25}\bar{\phi}_3 \end{aligned} \tag{10}$$

appearing on the right hand side (RHS) of equilibrium equations only relate to induced potential effects.

In order to consistently determine the field variables u, β and v, it is necessary to remove from the RHS of Eq. (9) the terms ϕ_u, ϕ_β, because of the initially required homogeneous form attribute of equilibrium relations. After have condensed the electrical relationships within the mechanical ones, integration of the resulting equation system leads to

$$\begin{Bmatrix} u \\ v \\ \beta \end{Bmatrix} = \Delta^{-1}\boldsymbol{\Lambda c} \tag{11}$$

where $\boldsymbol{c}$ is a vector of integration constants and

$$\boldsymbol{\Lambda} = \begin{bmatrix} \bar{A}_{22}x & -\frac{1}{2}\bar{A}_{12}x^2 & -\bar{A}_{12}x & \Delta & 0 & 0 \\ \frac{1}{2}\bar{A}_{12}x^2 & \frac{\Delta}{A_{33}}x - \frac{1}{6}\bar{A}_{11}x^3 & -\frac{1}{2}\bar{A}_{11}x^2 & 0 & -\Delta x & \Delta \\ -\bar{A}_{12}x & \frac{1}{2}\bar{A}_{11}x^2 & \bar{A}_{11}x & 0 & \Delta & 0 \end{bmatrix} \qquad \Delta = \bar{A}_{11}\bar{A}_{22} - \bar{A}_{12}^2 \tag{12}$$

with

$$\begin{aligned} \bar{A}_{11} &= A_{11} - C_1\frac{A_{14}^2}{A_{44}} - C_3\frac{A_{15}^2}{A_{55}} \\ \bar{A}_{12} &= A_{12} - C_1\frac{A_{14}A_{24}}{A_{44}} - C_3\frac{A_{15}A_{25}}{A_{55}} \\ \bar{A}_{22} &= A_{22} - C_1\frac{A_{24}^2}{A_{44}} - C_3\frac{A_{25}^2}{A_{55}} \end{aligned} \tag{13}$$

Imposition of the nodal displacements, as suggested by Fig. 4, yields

$$\boldsymbol{c} = \Delta\bar{\boldsymbol{\Lambda}}^{-1}\boldsymbol{d} \tag{14}$$

where

$$\bar{\boldsymbol{\Lambda}} = \begin{bmatrix} 0 & 0 & 0 & \Delta & 0 & 0 \\ 0 & 0 & 0 & 0 & 0 & \Delta \\ 0 & 0 & 0 & 0 & -\Delta & 0 \\ \bar{A}_{22}L_0 & -\frac{1}{2}\bar{A}_{12}L_0^2 & -\bar{A}_{12}L_0 & \Delta & 0 & 0 \\ \frac{1}{2}\bar{A}_{12}L_0^2 & \frac{\Delta}{A_{33}}L_0 - \frac{1}{6}\bar{A}_{11}L_0^3 & -\frac{1}{2}\bar{A}_{11}L_0^2 & 0 & -\Delta L_0 & \Delta \\ \bar{A}_{12}L_0 & -\frac{1}{2}\bar{A}_{11}L_0^2 & -\bar{A}_{11}L_0 & 0 & -\Delta & 0 \end{bmatrix} \qquad \boldsymbol{d} = \begin{Bmatrix} u_1 \\ v_1 \\ \theta_1 \\ u_2 \\ v_2 \\ \theta_2 \end{Bmatrix} = \begin{Bmatrix} u(0) \\ v(0) \\ -\beta(0) \\ u(L_0) \\ v(L_0) \\ -\beta(L_0) \end{Bmatrix} \tag{15}$$

Thus,

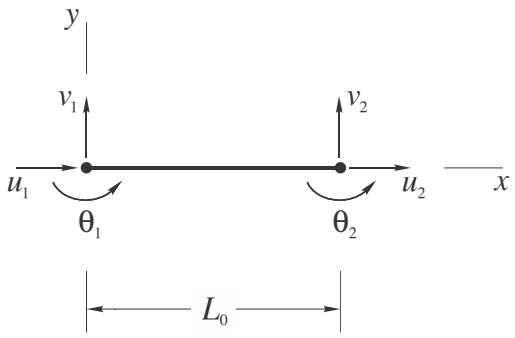

Figure 4. Element nodal displacements

$$\begin{Bmatrix} u \\ v \\ \beta \end{Bmatrix} = \boldsymbol{\Lambda}\bar{\boldsymbol{\Lambda}}^{-1}\boldsymbol{d} = \begin{bmatrix} \boldsymbol{N}_u^T \\ \boldsymbol{N}_v^T \\ \boldsymbol{N}_\beta^T \end{bmatrix}\boldsymbol{d} \tag{16}$$

with $\boldsymbol{N}_u$, $\boldsymbol{N}_v$, $\boldsymbol{N}_\beta$ being the interpolation functions that suitably provide superconvergent properties.

Following Meireles [30], the condensed mechanical-electrical equilibrium equation reads

$$\begin{aligned} \delta\boldsymbol{d}^T \int \left[\boldsymbol{N}_u'\left(\bar{A}_{11}\boldsymbol{N}_u'^T + \bar{A}_{12}\boldsymbol{N}_\beta'^T\right) + \boldsymbol{N}_\beta'\left(\bar{A}_{12}\boldsymbol{N}_u'^T + \bar{A}_{22}\boldsymbol{N}_\beta'^T\right) + A_{33}\left(\boldsymbol{N}_v' + \boldsymbol{N}_\beta\right)\left(\boldsymbol{N}_v'^T + \boldsymbol{N}_\beta^T\right)\right]dx\boldsymbol{d} \\ -\delta\boldsymbol{d}^T \int \left(q_x\boldsymbol{N}_u + q_y\boldsymbol{N}_v + \phi_u\boldsymbol{N}_u' + \phi_\beta\boldsymbol{N}_\beta'\right)dx - \delta\boldsymbol{d}^T\boldsymbol{r} = 0 \end{aligned} \tag{17}$$

The vector $\boldsymbol{r}$ collects nodal reaction forces. Since the components of $\delta\boldsymbol{d}$ are arbitrary and independent then

$$\boldsymbol{f} = \boldsymbol{p} + \boldsymbol{r} \tag{18}$$

where the vectors

$$\boldsymbol{f} = \boldsymbol{k}\boldsymbol{d} \qquad \boldsymbol{p} = \int_0^{L_0}\left(q_x\boldsymbol{N}_u + q_y\boldsymbol{N}_v + \phi_u\boldsymbol{N}_u' + \phi_\beta\boldsymbol{N}_\beta'\right)dx \tag{19}$$

gather the nodal internal and nodal equivalent forces, respectively.

The element stiffness matrix

$$\boldsymbol{k} = \int_0^{L_0}\left[\boldsymbol{N}_u'\left(\bar{A}_{11}\boldsymbol{N}_u' + \bar{A}_{12}\boldsymbol{N}_\beta'\right) + \boldsymbol{N}_\beta'\left(\bar{A}_{12}\boldsymbol{N}_u' + \bar{A}_{22}\boldsymbol{N}_\beta'\right) + \bar{A}_{33}\left(\boldsymbol{N}_v' + \boldsymbol{N}_\beta\right)\left(\boldsymbol{N}_v'^T + \boldsymbol{N}_\beta^T\right)\right]dx \tag{20}$$

can be analytically expressed as

$$\boldsymbol{k} = L_0^{-1}\begin{bmatrix} \bar{A}_{11} & 0 & -\bar{A}_{12} & -\bar{A}_{11} & 0 & \bar{A}_{12} \\ & 2\omega L_0^{-1} & \omega & 0 & -2\omega L_0^{-1} & \omega \\ & & k_1 & \bar{A}_{12} & -\omega & k_2 \\ & & & \bar{A}_{11} & 0 & -\bar{A}_{12} \\ & \text{sym} & & & 2\omega L_0^{-1} & -\omega \\ & & & & & k_1 \end{bmatrix} \qquad \omega = 6L_0\left(\frac{12}{A_{33}} + \frac{\bar{A}_{11}L_0^2}{\Delta}\right)^{-1} \tag{21}$$

with

$$\begin{aligned} k_1 &= \omega^2\left[\frac{\bar{A}_{11}L_0^2}{36\Delta^2}(4\Delta + \bar{A}_{12}^2) + \frac{\bar{A}_{22}}{A_{33}}\left(\frac{2\bar{A}_{11}}{3\Delta} + \frac{4}{A_{33}L_0^2} + \frac{1}{\bar{A}_{22}}\right)\right] \\ k_2 &= \omega^2\left[\frac{\bar{A}_{11}L_0^2}{36\Delta^2}(2\Delta - \bar{A}_{12}^2) - \frac{\bar{A}_{22}}{A_{33}}\left(\frac{2\bar{A}_{11}}{3\Delta} + \frac{4}{A_{33}L_0^2} - \frac{1}{\bar{A}_{22}}\right)\right] \end{aligned} \tag{22}$$

If the quantities q_x, q_y, ϕ_u and ϕ_β are constant along the element length then

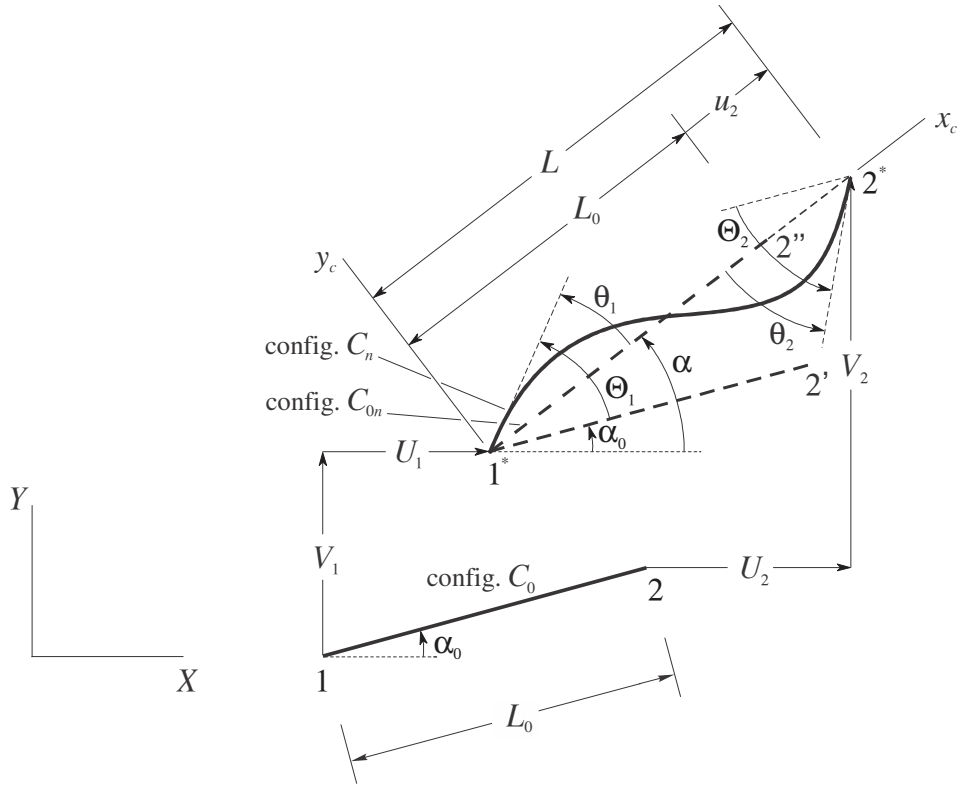

Figure 5. Element kinematics and coordinate systems

$$\boldsymbol{p} = \frac{1}{2}q_x L_0 \begin{Bmatrix} 1 \\ -\frac{1}{3\Delta}\bar{A}_{12}\omega \\ -\frac{1}{6\Delta}\bar{A}_{12}L_0\omega \\ 1 \\ \frac{1}{3\Delta}\bar{A}_{12}\omega \\ -\frac{1}{6\Delta}\bar{A}_{12}L_0\omega \end{Bmatrix} + \frac{1}{2}q_y L_0 \begin{Bmatrix} 0 \\ 1 \\ \frac{1}{6}L_0 \\ 0 \\ 1 \\ -\frac{1}{6}L_0 \end{Bmatrix} + \phi_u \begin{Bmatrix} -1 \\ 0 \\ 0 \\ 1 \\ 0 \\ 0 \end{Bmatrix} + \phi_\beta \begin{Bmatrix} 0 \\ 0 \\ 1 \\ 0 \\ 0 \\ -1 \end{Bmatrix} \tag{23}$$

3.2 Corotational formulation

The main idea in this formulation is to decompose the motion of the element into a rigid body and pure deformational parts, through the use of a reference system, which continuously rotates and translates with the element. The deformational response is captured at the level of the local reference frame, whereas the geometric nonlinearity induced by the large rigid-body motion, is incorporated in the transformation matrices relating local and global internal force vectors and tangent stiffness matrices. Assuming the pure deformation part to be small, a geometrical linear theory can be used in the local system. Using the notations defined in Fig. 5, the relations between the components of deformational nodal (corotational) displacements $\boldsymbol{d}_c = \lfloor \theta_1 \quad u_2 \quad \theta_2 \rfloor^T$ in the local frame and the components of global displacements $\boldsymbol{d}_g = \lfloor U_1 \quad V_1 \quad \Theta_1 \quad U_2 \quad V_2 \quad \Theta_2 \rfloor^T$ are [30]

$$u_2 = L - L_0 \qquad \theta_1 = \Theta_1 - (\alpha - \alpha_0) \qquad \theta_2 = \Theta_2 - (\alpha - \alpha_0) \tag{24}$$

where

$$\begin{aligned} L &= [(L_0 \cos\alpha_0 + U_2 - U_1)^2 + (L_0 \sin\alpha_0 + V_2 - V_1)^2]^{1/2} \\ \alpha &= \tan^{-1}[(L_0 \sin\alpha_0 + V_2 - V_1)(L_0 \cos\alpha_0 + U_2 - U_1)^{-1}] \end{aligned} \tag{25}$$

The transformation matrix **T** between the global displacements vector and the local deformational displacements vector is obtained by

$$\delta \boldsymbol{d}_c = \boldsymbol{T}\delta \boldsymbol{d}_g \qquad \boldsymbol{T} = \frac{\partial \boldsymbol{d}_c}{\partial \boldsymbol{d}_g} = \begin{bmatrix} \boldsymbol{T}_1^T \\ \boldsymbol{T}_2^T \\ \boldsymbol{T}_3^T \end{bmatrix} \tag{26}$$

with

$$\begin{aligned} \boldsymbol{T}_1^T &= L^{-1}\lfloor -\sin\alpha \quad \cos\alpha \quad L \quad \sin\alpha \quad -\cos\alpha \quad 0 \rfloor^T \\ \boldsymbol{T}_2^T &= \lfloor -\cos\alpha \quad -\sin\alpha \quad 0 \quad \cos\alpha \quad \sin\alpha \quad 0 \rfloor^T \\ \boldsymbol{T}_3^T &= L^{-1}\lfloor -\sin\alpha \quad \cos\alpha \quad 0 \quad \sin\alpha \quad -\cos\alpha \quad L \rfloor^T \end{aligned} \tag{27}$$

By equating the internal virtual work in the local and global systems, the equilibrium relationship between the local and global systems takes the form

$$\psi_g(\boldsymbol{d}_g) = \boldsymbol{f}_g - \boldsymbol{p}_g - \boldsymbol{r}_g = \boldsymbol{T}^T(\boldsymbol{f}_c - \boldsymbol{p}_c - \boldsymbol{r}_c) = \boldsymbol{T}^T\psi_c(\boldsymbol{d}_c) = \boldsymbol{0} \tag{28}$$

Assuming that the nodal reaction forces are independent of the element motion then $\partial \boldsymbol{r}_g/\partial \boldsymbol{d}_g = \boldsymbol{0}$, which implies

$$\boldsymbol{k}_t = \frac{\partial \boldsymbol{\psi}_g}{\partial \boldsymbol{d}_g} = \frac{\partial(\boldsymbol{T}^T\boldsymbol{f}_c)}{\partial \boldsymbol{d}_g} - \frac{\partial \boldsymbol{p}_g}{\partial \boldsymbol{d}_g} = \boldsymbol{T}^T\frac{\partial \boldsymbol{f}_c}{\partial \boldsymbol{d}_g} + \sum_{i=1}^{3} f_{ci}\frac{\partial \boldsymbol{T}_i}{\partial \boldsymbol{d}_g} - \frac{\partial \boldsymbol{p}_g}{\partial \boldsymbol{d}_g} \tag{29}$$

where f_{ci} are the components of

$$\boldsymbol{f}_c = \boldsymbol{k}_c\boldsymbol{d}_c = L_0^{-1}\begin{bmatrix} L_0k_1 & \bar{A}_{12} & L_0k_2 \\ & \bar{A}_{11} & -\bar{A}_{12} \\ \text{sym} & & L_0k_1 \end{bmatrix}\begin{Bmatrix} \theta_1 \\ u_2 \\ \theta_2 \end{Bmatrix} = \begin{Bmatrix} f_{c1} \\ f_{c2} \\ f_{c3} \end{Bmatrix} \tag{30}$$

According Meireles [30], the derivatives $\partial \boldsymbol{f}_c/\partial \boldsymbol{d}_g$, $\partial \boldsymbol{T}_i/\partial \boldsymbol{d}_g$ and $\partial \boldsymbol{p}_g/\partial \boldsymbol{d}_g$ can be written as

$$\frac{\partial \boldsymbol{f}_c}{\partial \boldsymbol{d}_g} = \boldsymbol{k}_c\boldsymbol{T} \qquad \frac{\partial \boldsymbol{T}_1}{\partial \boldsymbol{d}_g} = \frac{\partial \boldsymbol{T}_3}{\partial \boldsymbol{d}_g} = L^{-2}(\boldsymbol{T}_2\boldsymbol{z}^T + \boldsymbol{z}\boldsymbol{T}_2^T) \qquad \frac{\partial \boldsymbol{T}_2}{\partial \boldsymbol{d}_g} = L^{-1}\boldsymbol{z}\boldsymbol{z}^T \qquad \frac{\partial \boldsymbol{p}_g}{\partial \boldsymbol{d}_g} = \phi_u\frac{\partial \boldsymbol{T}_2}{\partial \boldsymbol{d}_g} \tag{31}$$

with

$$\boldsymbol{z} = \lfloor \sin\alpha \quad -\cos\alpha \quad 0 \quad -\sin\alpha \quad \cos\alpha \quad 0 \rfloor^T \tag{32}$$

Assemblage of the global equilibrium relations may be done, as usual, by

$$\boldsymbol{\Psi} = \sum \boldsymbol{\psi}_g = -\sum\left(\boldsymbol{k}_t\Delta \boldsymbol{d}_g\right) = -\boldsymbol{K}\Delta \boldsymbol{D} = \boldsymbol{F} - (\boldsymbol{P} + \boldsymbol{F}_{ext}) \tag{33}$$

where

$$\boldsymbol{K} = \sum \boldsymbol{k}_t \qquad \Delta \boldsymbol{D} = \sum \Delta \boldsymbol{d}_g \qquad \boldsymbol{F} = \sum \boldsymbol{f}_g \qquad \boldsymbol{P} = \sum \boldsymbol{p}_g \tag{34}$$

Equilibrium is then reached by vanishing the global residual forces $\boldsymbol{\Psi}(\boldsymbol{D}) = \boldsymbol{0}$, which can be iteratively solved by the Newton method.

4 Numerical Tests

Piezoelectric cantilevers beams in the sensing configuration are investigated. The length L of the beams is equal to 200 mm. They consist of a core layer (width $b = 25$ mm, thickness $h = 1$ mm) made of aluminum ($E = 70.3$ GPa, $\nu = 0.345$) and continuous layers of PZT-5H attached at the bottom (width $b_1 = b$, thickness $t_{p1} = h$) and top (width $b_3 = b$, thickness $t_{p3} = h$) of the host structure.

Material piezoelectric constitutive entries are [32]: $C_{11} = C_{22} = 126$ GPa, $C_{12} = 79.5$ GPa, $C_{13} = C_{23} = 84.1$ GPa, $C_{33} = 117$ GPa, $C_{66} = (C_{11} - C_{12})/2$, $C_{44} = C_{55} = 23$ GPa, $e_{31} = e_{32} = -6.5\ \text{C/m}^2$, $e_{33} = 23.3\ \text{C/m}^2$, $e_{15} = e_{24} = 17\ \text{C/m}^2$, $\xi_1 = \xi_2 = 15.05\ \text{nC}^2/\text{Nm}^2$ and $\xi_3 = 13.02\ \text{nC}^2/\text{Nm}^2$. The poling axis of the piezoelectric layers is aligned along the through-the-thickness direction.

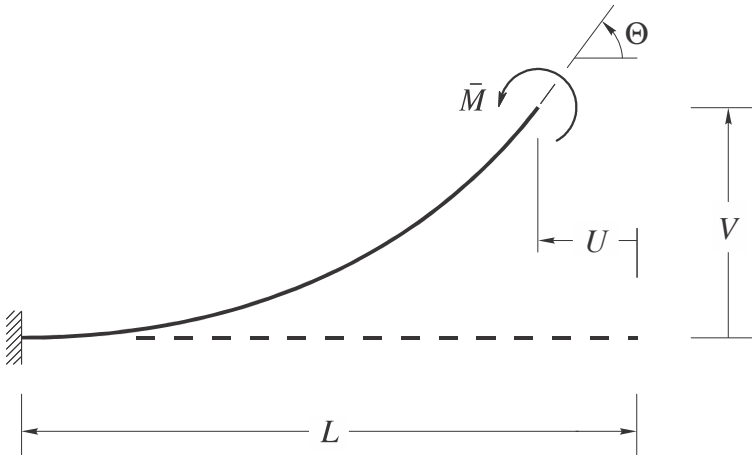

Figure 6. Cantilever beam subject to a moment-load

Nonlinear analyses are carried out employing a full Newton-Raphson solution strategy assuming as starting point the (natural) undeformed configuration. Converge criteria control are set by

$$max(e_D, e_F) \leq 10^{-3} \tag{35}$$

where

$$e_D^2 = \Delta\mathbf{D}_k^T\Delta\mathbf{D}_k/\mathbf{D}_{k+1}^T\mathbf{D}_{k+1} \qquad e_F^2 = \boldsymbol{\Psi}_k^T\boldsymbol{\Psi}_k/(\boldsymbol{P}+\boldsymbol{F}_{ext})_{k+1}^T(\boldsymbol{P}+\boldsymbol{F}_{ext})_{k+1} \tag{36}$$

At the k-th iteration, the quantity e_D is the ratio between the Euclidean norm of incremental-iterative nodal displacement $\Delta\mathbf{D}$ and the predicted one $\mathbf{D}$, e_F is the ratio between the Euclidean norm of residual force vector $\boldsymbol{\Psi}$ and the predicted vector $\boldsymbol{P} + \boldsymbol{F}_{ext}$. It is interesting note that all numerical pitfalls due to the huge difference magnitude order involving the mechanic and piezoelectric dielectric constants [2,33] are absent in the proposed formulation, because only mechanical degrees of freedom are concerned with the solution.

4.1 Cantilever beam with moment at free end

The cantilever beam of Fig. 6 is subjected to a moment $\bar{M}$ at the free end. The displacement and rotation components at the free end are identified by $U = -u(L)$, $V = v(L)$ and $\Theta = \theta(L)$ whose respective exact values U_e, V_e and Θ_e are given by Santos [10]. Table 1 presents these values for $\bar{M}L/2\pi K_1 =$ 0.5, 1, 1.5, 2 which correspond to the deformed beam in half turn (semicircle), one turn (circumference), one and a half turns, and two turns, respectively. Parameter K_1 is defined by

$$K_1 = K_2 + T_1\Omega_1 + T_4\Omega_3 \qquad \Omega_1 = \frac{T_3T_4+T_1T_5}{T_3^2-T_2T_5} \qquad \Omega_3 = \frac{T_1T_3+T_2T_4}{T_3^2-T_2T_5} \tag{37}$$

where

$$\begin{aligned} T_1 &= A_{24} + \frac{A_{12}A_{14}}{A_{11}} & T_2 &= A_{44} + \frac{A_{14}^2}{A_{11}} & T_3 &= \frac{A_{14}A_{15}}{A_{11}} \\ T_4 &= A_{25} + \frac{A_{12}A_{15}}{A_{11}} & T_5 &= A_{55} + \frac{A_{15}^2}{A_{11}} & K_2 &= A_{22} - \frac{A_{12}^2}{A_{11}} \end{aligned} \tag{38}$$

Table 2 shows the parameters $k_u = U/U_e$, $k_v = V/V_e$, $k_\theta = \Theta/\Theta_e$ for successively refined meshes. In geometrical terms, the discretization with only 2 elements makes the solution impossible. It is observed a good accuracy of the corotational models with 8 and 16 elements.

To evaluate the potential difference in a given element we proceed as follows. From Eq. (16),

$$\begin{Bmatrix} u \\ \beta \end{Bmatrix} = \begin{bmatrix} \boldsymbol{N}_u^T \\ \boldsymbol{N}_\beta^T \end{bmatrix}\boldsymbol{d} = \begin{bmatrix} \boldsymbol{N}_{uc}^T \\ \boldsymbol{N}_{\beta c}^T \end{bmatrix}\boldsymbol{d}_c \tag{39}$$

Table 1. Exact values U_e, V_e and Θ_e: cantilever beam with moment at free end

$\bar{M}L/2\pi K_1$	U_e/L	V_e/L	Θ_e
0.5	1	2/π	π
1	1	0	2π
1.5	1	2/3π	3π
2	1	0	4π

Table 2. Obtained results: cantilever beam with moment at free end

# Element	$\bar{M}L/2\pi K_1$	k_u	k_v	k_θ
2	0.5	1.000	1.111	1.000
	1	1.000	*	1.000
	1.5	-	-	-
	2	-	-	-
4	0.5	1.000	1.026	1.000
	1	1.000	*	1.000
	1.5	1.000	1.275	1.000
	2	1.000	*	1.000
8	0.5	1.000	1.007	1.000
	1	1.000	*	1.000
	1.5	1.000	1.060	1.000
	2	1.000	*	1.000
16	0.5	1.000	1.002	1.000
	1	1.000	**	1.000
	1.5	1.000	1.015	1.000
	2	1.000	***	1.000

$* V_{obtained} = 0$ $\quad ** V_{obtained} = 1 \times 10^{-8}$ $\quad *** V_{obtained} = 3 \times 10^{-8}$

where $\boldsymbol{N}_{uc}$ and $\boldsymbol{N}_{\beta c}$ are respectively $\boldsymbol{N}_u$ and $\boldsymbol{N}_\beta$ without the first, second and fifth components. Using the last two relations of Eq. (9),

$$\begin{Bmatrix} \bar{\phi}_1 \\ \bar{\phi}_3 \end{Bmatrix} = -\begin{bmatrix} \frac{A_{14}}{A_{44}} & \frac{A_{24}}{A_{44}} \\ \frac{A_{15}}{A_{55}} & \frac{A_{25}}{A_{55}} \end{bmatrix} \begin{Bmatrix} u' \\ \beta' \end{Bmatrix} = -\begin{bmatrix} \frac{A_{14}}{A_{44}} & \frac{A_{24}}{A_{44}} \\ \frac{A_{15}}{A_{55}} & \frac{A_{25}}{A_{55}} \end{bmatrix} \begin{bmatrix} \boldsymbol{N}'^T_{uc} \\ \boldsymbol{N}'^T_{\beta c} \end{bmatrix} \boldsymbol{d}_c \tag{40}$$

From Eq. (16)

$$\boldsymbol{N}'_{uc} = \frac{\omega}{\Delta L_0} \begin{Bmatrix} -\frac{\bar{A}_{12}}{2}(L_0 - 2x) \\ \frac{\Delta}{\omega} \\ -\frac{\bar{A}_{12}}{2}(L_0 - 2x) \end{Bmatrix} \qquad \boldsymbol{N}'_{\beta c} = \frac{\omega}{\Delta L_0} \begin{Bmatrix} \frac{2\Delta}{A_{33}L_0} + \frac{\bar{A}_{11}}{3}(2L_0 - 3x) \\ 0 \\ -\frac{2\Delta}{A_{33}L_0} + \frac{\bar{A}_{11}}{3}(L_0 - 3x) \end{Bmatrix} \tag{41}$$

Finally,

$$\begin{Bmatrix} \bar{\phi}_1 \\ \bar{\phi}_3 \end{Bmatrix} = -\frac{\omega}{\Delta L_0} \begin{bmatrix} \frac{A_{14}}{A_{44}} & \frac{A_{24}}{A_{44}} \\ \frac{A_{15}}{A_{55}} & \frac{A_{25}}{A_{55}} \end{bmatrix} \begin{Bmatrix} \frac{\Delta}{\omega}u_2 - \frac{\bar{A}_{12}}{2}(L_0 - 2x)(\theta_1 - \theta_2) \\ 0 \\ \left[\frac{2\Delta}{A_{33}L_0} + \frac{\bar{A}_{11}}{3}(2L_0 - 3x)\right]\theta_1 - \left[\frac{2\Delta}{A_{33}L_0} - \frac{\bar{A}_{11}}{3}(L_0 - 3x)\right]\theta_2 \end{Bmatrix} \tag{42}$$

where u_2, θ_1 and θ_2 are evaluated using Eq. (24). In this example, the obtained results

$$\frac{K_1}{\Omega_1 \bar{M}}\bar{\phi}_1 = \frac{K_1}{\Omega_3 \bar{M}}\bar{\phi}_3 = 1 \tag{43}$$

match the exact solution given by Santos [10] regardless of the mesh adopted.

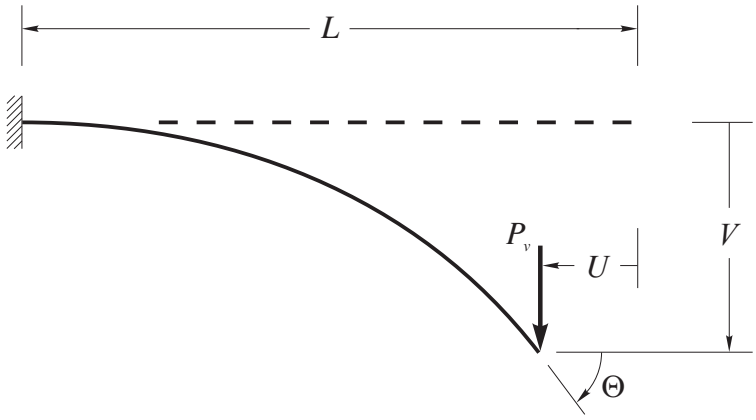

Figure 7. Cantilever beam subject to a transverse load

4.2 Cantilever beam with transverse load at free end

The beam analyzed in the first example is now considered subjected to the transverse force indicated in Fig. 7. The components of displacement and rotation at the free end are identified by $U = -u(L)$, $V = v(L)$ and $\Theta = \theta(L)$, whose respective exact values U_e, V_e and Θ_e are given in Table 3 for $P_v L^2/K_3 = 1, 4, 7, 10$. Parameter K_3 is defined by

$$K_3 = A_{22} - \frac{A_{24}^2}{A_{44}} - \frac{A_{25}^2}{A_{55}} \tag{44}$$

The table also contains, in its last column, the exact value of the parameter

$$\Phi = \frac{A_{44}L}{A_{24}}\bar{\phi}_1 = \frac{A_{55}L}{A_{25}}\bar{\phi}_3 \tag{45}$$

at the clamped end.

These exact values are determined by Santos [10] by elliptic integrals of first and second species, after neglecting the transverse shear deformation (beam Euler-Bernoulli) and the axial deformation of the beam axis. Thus, they are used herein only as reference values. Table 4 shows the obtained values of $k_u = U/U_e$, $k_v = V/V_e$, $k_\theta = \Theta/\Theta_e$, $k_1 = \Phi_1/\Phi_e$, $k_3 = \Phi_3/\Phi_e$ for successively refined meshes.

Table 3. Exact values U_e, V_e, Θ_e and Φ_e: cantilever beam with transverse load at free end

$P_v L^2/K_3$	U_e/L	V_e/L	Θ_e	Φ_e
1	0.056	0.302	0.461	0.944
4	0.329	0.670	1.121	2.684
7	0.473	0.767	1.335	3.690
10	0.555	0.811	1.430	4.450

5 Conclusions

The corotational finite element model developed for piezoelectric plane frames has its efficiency and large rotations capability proven by numerical examples. The element equation and all the linearizations required by the Newton-Raphson method are analytically and consistently formulated, including those related to the follower nature of the piezoelectrically induced loads. The voltage sensed by piezoelectric sensors, which are important data for their control of these structures, is completely different from the voltage predicted by linear model. The superconvergent linear element developed to describe the motion between C_{0n} and C_n has interpolation functions dependent on the mechanical properties of the material and the electrical properties of the sensor layers.

Table 4. Obtained results: cantilever beam with transverse load at free end

# Element	$P_v L^2/K_3$	k_u	k_v	k_θ	k_1	k_3
2	1	0.962	1.007	1.006	1.001	1.003
	4	0.990	1.031	1.026	0.997	1.004
	7	1.014	1.041	1.032	0.982	0.993
	10	1.023	1.046	1.033	0.964	0.978
4	1	0.990	1.002	1.001	1.000	1.001
	4	0.998	1.007	1.006	0.999	1.003
	7	1.000	1.009	1.006	0.997	1.003
	10	1.002	1.011	1.007	0.994	1.003
8	1	0.998	1.001	1.000	1.000	1.000
	4	1.000	1.002	1.001	0.999	1.001
	7	1.000	1.003	1.001	0.998	1.002
	10	1.000	1.003	1.002	0.997	1.002
16	1	1.000	1.000	1.000	1.000	1.000
	4	1.000	1.001	1.000	0.999	1.001
	7	1.000	1.001	1.000	0.999	1.001
	10	1.000	1.001	1.000	0.998	1.001

One advantage of the proposed element is that it can be treated by the corotational algorithm as being purely mechanical and, thus, any additional complexity brought by piezoelectricity is locally treated. For instance, all numerical pitfalls due to the huge difference magnitude order involving the mechanic and piezoelectric dielectric constants are absent in the proposed formulation.

References

[1] D. J. Leo. *Engineering analysis of smart material systems*. John Wiley, 2007.
[2] E. L. Cardoso and J. S. Fonseca. An incremental Lagrangian formulation to the analysis of piezo-electric bodies subjected to geometric non-linearities. *International Journal for Numerical Methods in Engineering*, vol. 59, n. 7, pp. 963–987, 2004.
[3] S. Q. Zhang, Y. X. Li and R. Schmidt. Active shape and vibration control for piezoelectric bonded composite structures using various geometric nonlinearities. *Composite Structures*, vol. 122, pp. 239–249, 2015.
[4] A. Mukherjee and A. S. Chaudhuri. Piezolaminated beams with large deformations. *International Journal of Solids and Structures*, vol. 39, n. 17, pp. 4567–4582, 2002.
[5] A. Mukherjee and A. S. Chaudhuri. Nonlinear dynamic response of piezolaminated smart beams. *Computers and Structures*, vol. 83, n. 15–16, pp. 1298–1304, 2005.
[6] S. Kapuria and N. Alam. Zigzag theory for buckling of hybrid piezoelectric beams under electromechanical loads. *International Journal of Mechanical Sciences*, vol. 46, n. 1, pp. 1–25, 2004.
[7] S. Cescotto, F. Frey and G. Fonder, 1979. Total and updated Lagrangian descriptions in non-linear structural analysis: a unified approach. In: R. Glowinski *et al.* (ed.), *Energy methods in finite element analysis*, pp. 283–296.
[8] L. E. Malvern, *Introduction to the mechanics of a continuous medium*. Prentice-Hall, 1969.
[9] D. S. Chandrasekharaiah and L. Debnath. *Continuum mechanics*. Academic Press, 1994.
[10] R. R. F. Santos. Vigas piezelétricas sob pequenas deformações mas grandes rotações: uma formulação lagrangiana total. MSc thesis, Instituto Tecnológico de Aeronáutica, 2018.
[11] J. H. Argyris, 1964. Recent advances in matrix methods of structural analysis. In: A. Ferri *et al.* (ed.), *Progress in aeronautical sciences*.
[12] J. H. Argyris, H. Balmer, J. Doltsinis, P. C. Dunne, M. Haase, M. Kleiber, G. A. Malejannakis, H. P. Mlejnek, M. Müller and D. W. Scharpf. Finite element method – the natural approach. *Computer Methods in Applied Mechanics and Engineering*, vol. 17–18, pp. 1–106, 1979.
[13] G. Wempner. Finite elements, finite rotations and small strains of flexible shells. *International Journal of Solids and Structures*, vol. 5, n. 2, pp. 117–156, 1969.

[14] T. Belytschko and B. J. Hsieh. Non-linear transient finite element analysis with convected co-ordinates. *International Journal for Numerical Methods in Engineering*, vol. 7, n. 3, pp. 225–271, 1973.
[15] C. Oran, Tangent stiffness in plane frames. *Journal of the Structural Division*, vol. 99, pp. 973–985, 1973.
[16] C. Oran, Tangent stiffness in plane frames. *Journal of the Structural Division*, vol. 99, pp. 987–1001, 1973.
[17] C. Oran and A. Kassimali. Large deformation of framed structures under static and dynamic loads. *Computers and Structures*, vol. 6, n. 6, pp. 539–547, 1976.
[18] T. Belytschko and L. W. Glaum. Applications of higher order corotational stretch theories to nonlinear finite element analysis. *Computers and Structures*, vol. 10, n. 1–2, pp. 175–182, 1979.
[19] K. J. Bathe. *Finite element procedures*. Prentice-Hall, 1996.
[20] G. Rama, D. Marinković and M. Zehn. Piezoelectric co-rotational 3-node shell element. *American Journal of Engineering and Applied Sciences*, vol. 9, n. 4, pp. 902–912, 2016.
[21] D. Marinković and G. Rama. Co-rotational shell element for numerical analysis of laminated piezoelectric composite structures. *Composites Part B: Engineering*, vol. 125, pp. 144–156, 2017.
[22] Z. Friedman and J. B. Kosmatka. An improved two-node Timoshenko beam finite element. *Computers and* Structures, vol. 47, n. 3, pp. 473–481, 1993.
[23] M. Eisenberger. Derivation of shape functions for an exact 4-d.o.f. Timoshenko beam element. *Communications in Numerical Methods in Engineering*, vol. 10, n. 9, pp. 673–681, 1994.
[24] J. N. Reddy. On locking-free shear deformable beam finite elements. *Computer Methods in Applied Mechanics and Engineering*, vol. 149, n. 1–4, pp. 113–132, 1997.
[25] D. Marinković, H. Köppe and U. Gabbert. Aspects of modeling piezoelectric active thin-walled structures. *Journal of Intelligent Material Systems and Structures*, vol. 20, n. 15, pp. 1835–1844, 2009.
[26] A. Butz, S. Klinkel and W. Wagner. A geometrically and materially non-linear piezoelectric three-dimensional-beam finite element formulation including warping effects. *International Journal for Numerical Methods in Engineering*, vol. 76, n. 5, pp. 601–635, 2008.
[27] A. A. Khdeir, E. Darraj and O. J. Aldraihem. Free vibration of cross ply laminated beams with multiple distributed piezoelectric actuators. *Journal of Mechanics*, vol. 28, n. 1, pp. 217–227, 2012.
[28] M. A. Elshafei, M. R. Ajala and A. M. Riad. Modeling and analysis of smart Timoshenko beams with piezoelectric materials. *International Journal of Engineering and Innovative Technology*, vol. 3, n. 11, pp. 21–33, 2014.
[29] L. N. Sulbhewar and P. Raveendranath. An accurate novel coupled field Timoshenko piezo-electric beam finite element with induced potential effects. *Latin American Journal of Solids and Structures*, vol. 11, n. 9, pp. 1628–1650, 2014.
[30] J. G. S. A. Meireles. Um modelo corrotacional de elementos finitos para pórticos planos piezelétricos. MSc thesis, Instituto Tecnológico de Aeronáutica, 2019.
[31] I. M. Gelfand, S. V. Fomin. *Calculus of variations*. Dover, 2000.
[32] J. Yang. *An introduction to the theory of piezoelectricity*, 2nd ed. Springer, 2018.
[33] H. Qi, D. Fang and Z. Yao. FEM analysis of electro-mechanical coupling effects of piezoelectric materials. *Computational Materials Science*, vol. 8, n. 4, pp. 283–290, 1997.